PCCP

Accepted Manuscript

This article can be cited before page numbers have been issued, to do this please use: E. D. Cantero, L. M. Solis, Y. Tong, J. D. Fuhr, M. L. Martiarena, O. Grizzi and E. Sanchez, *Phys. Chem. Chem. Phys.*, 2017, DOI: 10.1039/C7CP02949G.

View Article Online
DOI: 10.1039/C7CP02949G

Physical Chemistry Chemical Physics

ARTICLE

Growth of germanium on Au(111): formation of germanene or intermixing of Au and Ge atoms?

Received 00th January 20xx,
Accepted 00th January 20xx

DOI: 10.1039/x0xx00000x

www.rsc.org/

Esteban D. Cantero[a], Lara M. Solis[b], Yongfeng Tong[c], Javier D. Fuhr[a], María Luz Martiarena[a], Oscar Grizzi[a] and Esteban A. Sánchez[a]

We studied the growth of Ge layers on Au(111) under ultra-high vacuum conditions from the submonolayer regime up to a few layers with Scanning Tunneling Microscopy (STM), Direct Recoiling Spectroscopy (DRS) and Low Energy Electron Diffraction (LEED). Most STM images for the thicker layers are consistent with a commensurate 5 x 8 arrangement. The high surface sensitivity of TOF-DRS allows to confirm the coexistence of Au and Ge atoms in the top layer for all stages of growth. An estimation of the Au to Ge ratio at the surface of the thick layer gives about 1 Au atom per 2 Ge ones. When the growth is carried out at sample temperatures higher than about 420 K, a fraction of the deposited Ge atoms migrates into the bulk of Au. This incorporation of Ge into the bulk reduces the growth rate of the Ge films, making more difficult to obtain films thicker than few layers. After sputtering the Ge/Au surface, the segregation of bulk Ge atoms to the surface occurs for temperatures ≥ 600 K. The surface obtained after segregation of Ge reaches a stable condition (saturation) with a nxn symmetry with n of the order of 14.

A. Introduction:

Graphene, silicene and germanene are part of the new family of 2-D materials that attracted much attention recently due to their novel properties[1,2] and possible applications.[3-5] The difficulties associated to creating a gap in graphene encouraged more studies based on Si,[6-8] Ge,[9-18] on new methods of fabrication,[19] and on other materials such as transition metal dichalcogenides.[20,21] Among the specific properties of each system, the expected buckled honeycomb structure of silicene and germanene should increase the reactivity of the layer to adsorb atoms and molecules making these systems good candidates for sensor and other applications.[17] These films are always grown or synthesized on surfaces which ideally should play little or no role in the film properties. For that reason a lot of effort is paid at present to find substrates that will allow the growth of the ultra-thin film preserving all its desired properties. In the report by Acun et al[18] all the attempts to synthesize germanene on metallic surfaces are reviewed up to 2015. In that work the authors also proposed the use of wide band gap materials as substrates in order to reduce the hybridization of the electronic states of germanene and the metallic substrate. In particular, a recent DFT study[22] for germanene and silicene on different surfaces states that the Dirac cone would be preserved for germanene on Ag and on Au, while it would be destroyed for silicene and for germenene on Al, Pt and Ir. This theoretical result is in agreement with the recent experiments by Dávila and Le Lay[9,10] where Ge films having a thickness of a few monolayers grown on Au(111) presented Dirac cones, thus placing this system among the few 2-D Dirac materials known up to date. In those initial works[9,10] it was suggested that the interaction between Au substrate atoms and Ge is strong but limited to the submonolayer regime, or up to completion of the first monolayer, on top of which the true germanene grows[9]. This incorporation or mixing of substrate atoms into the Ge layer is not limited to Au substrates; a similar behaviour has been proposed for other films[23] and at present is a subject of debate and importance due to the effect that this may have on the family of new materials.

In order to outline the role of the substrate and characterize in detail the film at all stages a combination of very sensitive surface techniques[23] is highly desirable, and in particular a technique such as direct recoil spectroscopy combined with Time of Flight analysis (TOF-DRS)[24] which is sensitive to all elements and can delineate unambiguously between top layer atoms and subsurface atoms becomes very powerful. In this work we studied the growth of Ge layers on Au(111) for different sample temperatures and evaporation rates and followed in situ the growth with TOF-DRS and LEED. At all stable conditions we recorded LEED patterns that were considered the fingerprints of each structure according to refs.

[a] Centro Atómico Bariloche, Comisión Nacional de Energía Atómica CNEA, Consejo Nacional de Investigaciones Científicas y Técnicas CONICET. Instituto Balseiro, Universidad Nacional de Cuyo.
[b] Instituto Balseiro, Universidad Nacional de Cuyo.
[c] Université de Paris Sud, Institut des Sciences Moléculaires d'Orsay, UMR 8214 CNRS Université Paris Sud, Université Paris Saclay, Bâtiment 351, Orsay 91405, France. Synchrotron SOLEIL - L'Orme des Merisiers, Saint-Aubin - BP 48, 91192 GIF-sur-YVETTE CEDEX, France.

† Electronic Supplementary Information (ESI) available: Additional information on TOF-DRS spectra with Ne projectiles, LEED patterns, Coexistence of Au and Ge atoms in the same atomic layer, STM images, and DFT calculations.

View Article Online
DOI: 10.1039/C7CP02949G

[9] and [10], and for some specific conditions we studied the crystallography by means of STM images. The images for the thicker films were consistent with an arrangement of atoms in a 5x8 unit cell. We found that for all the cases studied, from submonolayer to few layers, an amount of Au atoms was present at the top layer, following a symmetry different from that of the bulk. For adsorptions carried out with the sample above 420 K there was incorporation of Ge into the bulk. Segregation of this Ge to the surface was evidenced after annealing above 600 K. This segregated surface presented a well ordered surface with a nxn symmetry with n of the order of 14.

B Experiment:

The experiments were carried out in two separate UHV chambers working at 10^{-10} Torr, having both facilities for film growth and in situ characterization by LEED. One of the chambers is connected to an ion accelerator for TOF-DRS measurements and the other has a variable temperature STM. The LEED optics in the TOF-DRS system has amplification by a channelplate, which allows observing better details in the diffraction pattern with lower incident currents. The Au surface was prepared by cycles of 1.5 keV Ar^+ sputtering and annealing at temperatures around 750 K, and then characterized in both cleanliness and surface order by TOF-DRS.

In TOF-DRS, the samples are bombarded by a pulsed beam of a few keV Ar^+ or Ne^+ ions at different incidence angles, here indicated with respect to the surface plane. A time-of-flight analysis of the ejected particles is then performed by using a detector (Channel electron multiplier) placed at the end of a 1.76 m long time-of-flight drift tube set at 45° with respect to the incident beam direction. By measuring the time required for a particle to travel that known distance, its velocity is calculated. After that, the mass of the detected particle can be determined by using the equations of a single collision process[25]. Since different masses leave the surface at different energies (velocities), the TOF spectra will present peaks that can be assigned to projectiles scattered off target atoms, or to target atoms recoiled by the incoming projectile. [24, 25] At the scattered energies (some keV energy range), both neutral and ion scattered particles are detected with similar sensitivity thus avoiding uncertainties due to the electron exchange processes that can take place at the surface.

The incident beam current density, measured with a Faraday cup at the end of the beam line, was ~1 nA/mm^2 without pulsing the beam. During TOF acquisition, the mean pulsed beam current is approximately 10^3 times lower than that of the continuous beam. Thus, for a typical TOF spectrum of 5 minutes of acquisition time, the fluence reaches $2x10^{11}$ ions/cm^2, which ensures that the damage imparted during analysis is negligible.[24] This agrees with the fact that no changes were observed neither in the TOF-DRS spectrum nor in the LEED patterns after acquisition of several consecutive spectra.

The second UHV chamber (base pressure ~10^{-10} Torr) was equipped with a variable temperature STM (model VT AFM 25 DRH) and a LEED system, both from Omicron NanoTechnology.[26]

The STM images were acquired in a constant current mode with the sample held at room temperature. The bias voltages V_S indicated in the manuscript are applied to the sample with respect to the STM tip; i.e., positive (negative) V_S values correspond to unoccupied (occupied) state images. The tips were produced by electrochemical etching of a 0.25 mm diameter tungsten wire in a NaOH solution. The images were processed using the WS×M software.[27] Lateral thermal drifts were corrected by using the procedure described in ref. [28].

The Au(111) single crystal was obtained from Mateck GmbH.[29] The temperature was measured by means of S or K thermocouples attached to the different sample holders.

For the evaporations we used a Knudsen type evaporator working at low fluence, which allowed keeping the chamber pressure in the low 10^{-9} Torr range during evaporations, and with a growth rate that was varied in the range of 1 to 2 monolayers per hour, similar to the rate used in ref. [9]. We tested different evaporation methods: with the sample at 470 K, at room temperature, with and without post-annealing at 520 K, and for several evaporation rates. In all cases the resulting layer was analysed with LEED, and with TOF-DRS (or with Auger Electron Spectroscopy in the STM chamber).

C Results and Discussion:

C1 Clean Surface: In order to show how TOF-DRS is used to obtain information about the last atomic layer of the Ge/Au(111) system we describe first the clean Au surface. In Fig. 1 we present the characteristic LEED pattern (panel (a)) and the corresponding STM image (panel (b)) of the herringbone reconstruction. TOF-DRS spectra recorded with 4.2 keV Ar^+ ions along the $[\bar{1}01]$ and $[\bar{2}11]$ at 20° incidence are shown in panel (c). The more intense peaks (Ar-Au) at the left side of the spectrum correspond to Ar scattering off Au; the intensity is higher along the more compact $[\bar{1}01]$ direction. The other peak (Au) corresponds to Au recoils that are seen only along the more open $[\bar{2}11]$ direction.

Shadowing and/or focussing effects are stronger for quasi direct recoiling processes than for projectile scattering[25] and are therefore very sensitive to changes at the top layer crystallography. In particular, shadowing effects for Ar^+ at 4.2 keV precludes observation of Au recoils along other, more compact directions. Even along the $[\bar{2}11]$ direction the peak is not truly due to direct recoiling (single collisions), as it is affected by focussing which enhances its intensity and places the Au peak maximum at a lower TOF position than that corresponding to a true direct recoil process. For other lighter projectiles at higher energies (such as Ne) the shadowing effects are less prominent and some Au recoil contribution can be observed at all azimuthal directions. This point is further discussed in the supplementary information. The presence or the complete absence of Au recoils and their TOF position at specific directions are the signs of the well-ordered Au(111)

View Article Online
DOI: 10.1039/C7CP02949G

atomic structure. Reconstructions or adatoms, as we see further below, modify these features.

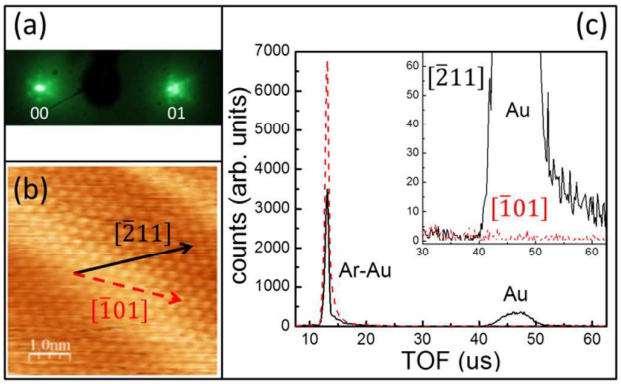

Fig. 1: (a) LEED pattern showing the characteristic 00 and 01 spots of the 22x√3 herringbone reconstruction of the clean Au(111) surface. (b) 5x5 nm^2 STM image recorded with V_S= -0.1 V and I_T = 10 nA. The main crystal surface directions are indicated in the atomic resolved image. (c) TOF-DRS spectra recorded with 4.2 keV Ar^+ ions along the [$\bar{1}$01] and [$\bar{2}$11] directions at 20° incidence.

C2 Growth of Ge layers: The growth of the Ge layer is well monitored by TOF-DRS performed "in situ" because it is fast (typically each spectrum is taken in the range of 2 to 5 minutes), non-destructive, and not affected by the evaporation or the heating of the sample, so all the growth parameters remain unchanged during acquisition. The growth is monitored by following the changes in the clean surface peaks plus the new ones due to Ge (both projectile scattering from Ge and Ge recoils).

Figures 2 (a) and (c) show a set of spectra taken along the open azimuthal direction [$\bar{2}$11] for different exposure times. Panel (a) shows the region of Ar scattering off Au and Ge atoms, and panel (c) the region of Au and Ge recoiling. Panels (b) and (d) show the intensities of the corresponding peaks. For this evaporation the sample temperature was set at 470 K, following the recipe of ref. [9] The spectrum at the bottom was taken after performing an annealing of the surface at 520 K.[9] With increasing evaporation time we observe a decrease of the Ar scattering off Au (Ar-Au) accompanied by an increase of the Ar scattering off Ge (Ar-Ge). In correspondence with the scattering features, the Au recoil peak also decreases and a new Ge recoil peak becomes observable (panels (c) and (d)). All these features become stable around 30 min of evaporation time, which is assumed to be the completion of the first monolayer. For evaporation times between 10 and 20 min, the Ge peak appears stronger because in the not yet completed first monolayer the shadowing effects are less important than in the full monolayer. Longer exposures produce changes in the shape of the Ge recoiling peak which becomes a smaller, more shoulder type, less-defined peak. These changes in the Ge peak reveal an increase in the shadowing of the trajectories due to the evolution of the surface crystallography.

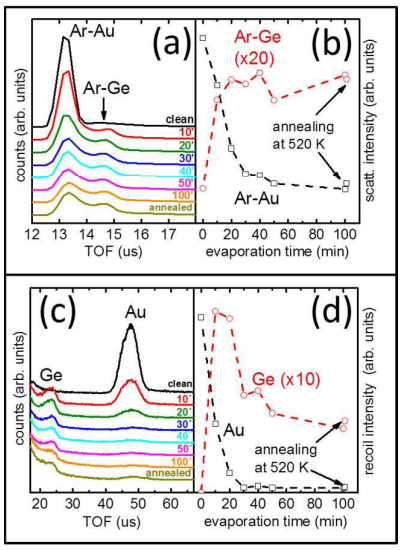

Fig. 2 TOF-DRS spectra recorded with 4.2 keV Ar^+ ions along the [$\bar{2}$11] direction at 20° incidence, during Ge deposition. (a) and (b) TOF region for Ar scattering peaks and their corresponding integration area. (c) and (d) same as (a) and (b) for the recoiling peaks.

Fig. 3 (a) shows the LEED pattern obtained after 30 min of evaporation. When the evaporation is stopped at this time and the surface is immediately annealed at 520 K, the LEED pattern changes as shown in Fig. 3 (b), reproducing the pattern presented in ref. [10] for one monolayer. Additional sets of LEED patterns taken at different electron energies prior and after annealing are shown in figures SI-3 and SI-4 of the Supp. Inf., respectively. When the evaporation is performed continuously up to 100 min and then the surface is annealed at 520 K, a new LEED pattern becomes observable (Fig. 3 (c)). This new pattern is similar to that proposed in ref. [9] for the germanene multilayer.

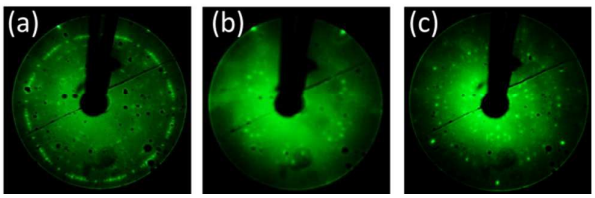

Fig. 3 LEED patterns after (a) 30 min Ge deposition, (b) 30 min Ge deposition with post annealing at 520 K, and (c) 100 min Ge deposition followed by post annealing at 520 K. Electrons energies were (a) 56.6 eV, (b) 55 eV and (c) 79.4 eV.

TOF-DRS spectra taken along the closed packed direction [$\bar{1}$01] (Fig. 4 (a)) reveal the appearance of a Au recoil peak since the lowest adsorption times (10 min) corresponding to a fraction of a Ge monolayer. This confirms the proposal of having a mixed Ge-Au layer as interface,[9,10] since the only possibility of measuring a Au recoil peak along this direction (not observed in the clean surface) is either by a reconstruction of the Au substrate surface to expose Au atoms or by some migration of Au atoms into the Ge layer. Determination of the coexistence of Au and Ge atoms in the same atomic layer is a critical issue, and few techniques

View Article Online
DOI: 10.1039/C7CP02949G

(including TOF-DRS) have enough sensitivity to provide clear evidences of this phenomenon. In the Supp. Inf. we further develop this point to show that this is specific of the Ge/Au system.

The intensity of the recoil peaks is plotted versus evaporation time in Fig. 4(b). Here we note a strong crystallographic effect in the Ge recoils for low exposures, they are seen better along the open $[\bar{2}11]$ direction and appear almost unnoticed along the $[\bar{1}01]$ direction, thus having the same dependence observed for Au recoils in the clean surface. This dependence is lost at high exposures where we observe that both Ge and Au recoils are detected with similar (low) intensity along all azimuthal directions. Another important result is the clear observation of the Au recoil peak along the $[\bar{1}01]$ direction even for the longer exposures, equivalent to three or more times the needed to form one monolayer. This is a confirmation of the presence of Au atoms at the top layer of the Ge film. The post-annealing of the films at this condition introduces changes in the LEED patterns and also in the shape of the Ge recoil peaks, but for all these cases, before and after the post annealing there was a clear Au recoil peak due to Au atoms at the top-most layer.

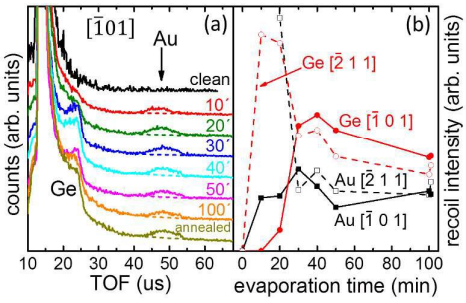

Fig. 4 TOF-DRS spectra recorded with 4.2 keV Ar^+ ions along the $[\bar{1}01]$ direction at 20° incidence during Ge deposition (a), and the intensity of the recoil peaks (b) compared (in the same scale) to the recoil intensity measured along the $[\bar{2}11]$. Backgrounds for the Au recoiling peaks are indicated with dashed lines.

We performed similar studies for evaporations at higher and at lower evaporation rates, and with different projectiles (Ne), with different energies, and in particular at grazing incidence which becomes more surface sensitive, and for all cases there was a clear evidence for Au atoms at the top-most surface layer. Other TOF-DRS examples with Ne projectiles are presented in the Supp. Inf. Note that if this peak was initially coming from a Au surface reconstruction, it should disappear for a sufficiently thick Ge layer (one pure Ge monolayer should be sufficient to preclude observation of Au recoils). The permanence of the Au recoil peak for all conditions (even for grazing angles as low as 5°, see Supp. Inf.) is a proof of the existence of Au atoms at the top-most layer.

Another point of interest is if the Au atoms detected at the top could be acting as a surfactant layer, i.e., present only on the top layer, or if they are distributed in the whole layer. To test this point we tried to grow a relatively thick layer of Ge, but due to migration of Ge into bulk, which is described in the next section, we could not grow layers thicker than about three - four monolayers.[30] TOF-DRS studies carried out versus sputtering time on these samples were compatible with the presence of Au in the whole layer. However, this is not a conclusive answer because the layers studied were not thick enough and some mixing might be induced by the sputtering process with the 800 eV Ar continuous beam.

Contrary to other systems where the adsorbates protrude above the substrate layer at low coverages, here the growth of Ge is locally ordered already at small coverages, forming an initial phase with Ge and Au atoms presenting similar shadowing effects in the recoiling trajectories. In Fig. 5 we present a comparison of TOF-DRS spectra for Ge and Se adsorptions carried out independently, on similarly prepared Au(111) surfaces and at approximately the same coverage. It corresponds to coverages well in the submonolayer regime, with the Au recoil peak along the $[\bar{2}11]$ direction clearly observable (about 10 min of evaporation time). The Se peak appears clean, narrow, at the TOF position corresponding to a true direct recoil event and very similar along both directions. This is a typical case of adsorbates lying above the substrate at low coverages. On the other hand, the Ge recoil peak appears broad and shifted to lower TOF positions, and presenting a strong dependence on crystallography; similar to that observed for Au atoms in a clean Au(111) surface. This would be consistent with Ge atoms occupying substitutional Au sites at the beginning of the adsorption. LEED measurements also show that the adsorption is ordered since the beginning and passing through different patterns before the first monolayer is completed.

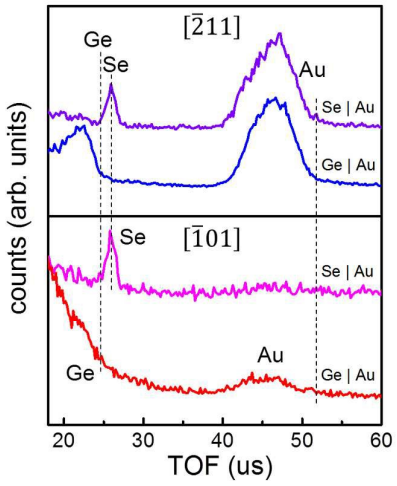

Fig. 5 TOF-DRS spectra recorded with 4.2 keV Ar^+ ions at 20° incidence for Se and Ge deposition on Au(111). Upper panel for the $[\bar{2}11]$ azimuthal direction. Lower panel for the $[\bar{1}01]$ azimuthal direction. The black vertical dashed lines indicate from left to right, the TOF position of the true direct recoil peak of Ge, Se and Au, respectively.

DFT calculations are in agreement with this scenario. For an isolated Ge atom (represented in the calculation by one Ge in a 3x3 Au(111) slab), the substitutional Au sites are

View Article Online
DOI: 10.1039/C7CP02949G

energetically favorable (by ~30 meV) compared to the lowest-energy adsorbed site. From calculations performed with different proportion of Ge atoms in different unit cells for the submonolayer coverage we found several configurations with similar adsorbed energy per Ge atom (Table S1 in Supp. Inf.). All of them consist of a Ge-Au alloy layer with a triangular array but more compact than the ideal Au(111).

The determination of the Ge to Au ratio at the surface is important information to compare with the proposed models, and, ideally, can be obtained from TOF-DRS spectra by integration of the recoiling peaks, correcting their intensities by their corresponding cross sections, provided that there are no shadowing or focusing effects. Unfortunately, as we mentioned before, the results obtained with Ar bombardment are very dependent on the polar or azimuthal incident conditions due to both shadowing and focussing; this makes the technique very sensitive to the top layer and to changes in it, but it makes very difficult the elemental quantification. In order to get a rough estimation of the ratio of Ge to Au atoms we performed measurements with Ne^+ ions (Supp. Inf.) at higher energies (12 keV) in conditions where the effect of shadowing and blocking is reduced (16^o incidence angle along the $[\bar{2}11]$ direction). The Ge/Au ratio obtained from these measurements, corresponding to the thick Ge layer (exposures around 100 min), is around 2, with values in the range from 1.5 to 3. Therefore, a honeycomb structure with two Au atoms and four Ge atoms on the top layer would be a possibility that deserves to be checked by calculations. This is a difficult task to perform because this layer is sitting on the Ge/Au(111) intermediate layer for which there is little information.

In the following we discuss the STM images obtained for the thick Ge layer. In Fig. 6 we present an example of the most frequently observed STM images after adsorption of the Ge layer. In panels (a) and (b) of Fig. 6 the STM images with different magnifications show that the arrangement is produced along the $[\bar{1}01]$ Au direction, as indicated in panel (a) with a red dashed line. The STM image looks similar to that obtained in ref. [11], where the growth of the Ge layers was performed in an electrochemical cell. A close inspection of the STM images show that the honeycomb structure expected for the germanene layer is hard to identify, and that the correlation with the LEED pattern presented in Fig. 3(c) is not easily discernible and requires discussion.

In order to find the unit cell size and symmetry we consider the STM image (Fig. 6, panel (a)) as composed by a single domain with a Fast Fourier Transformation (2D-FFT) that is shown in panel (c). We propose a superstructure with a unit cell of 5x8, as shown by the white box in panel (a). Panel (d) shows the simulation with LEEDPat software[31] of the 5x8 structure together with the brighter spots resulting from the 2D-FFT of panel (c) that fit the simulation (red circles). To compare with the experimental LEED pattern one has to sum all the patterns produced by the possible different domains with 5x8 symmetry. This comparison is presented in Fig. 7, which shows a good agreement between the simulation and the experimental LEED pattern. Not all the simulated spots are seen in the 2D-FFT pattern, neither in the experimental LEED because their presence is determined by the position of the atoms within the cell, which at present is unknown; however we expect that these new findings will be useful for future first principle calculations.

With less frequency we observed images (shown in Fig. SI-5 of the Supp. Inf.) formed by hexagonal bright spots arranged at 0.35 nm distance presenting a (6x6) moiré type pattern. The distance between bright spots does not correspond neither with the Au substrate atoms nor with the pure germanene layer.

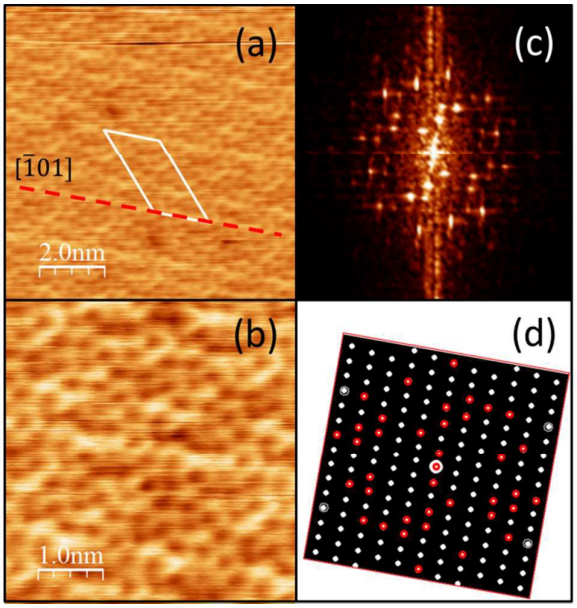

Fig. 6 (a) and (b) STM images acquired with V_S= -0.1 V and I_T = 3 nA, after deposition of the thick Ge layer. The red dashed line corresponds to the $[\bar{1}01]$ Au direction and the white box to the proposed 5x8 unit cell. (c) 2D-FFT pattern of image (a) calculated by WSxM software[27] and (d) LEED pattern calculated by LEEDPat 4.1 software[31] for a single domain of a 5x8 structure. The red spots are those that can be easily found in the 2D-FFT pattern of panel (c) that coincide with spots of panel (d).

View Article Online
DOI: 10.1039/C7CP02949G

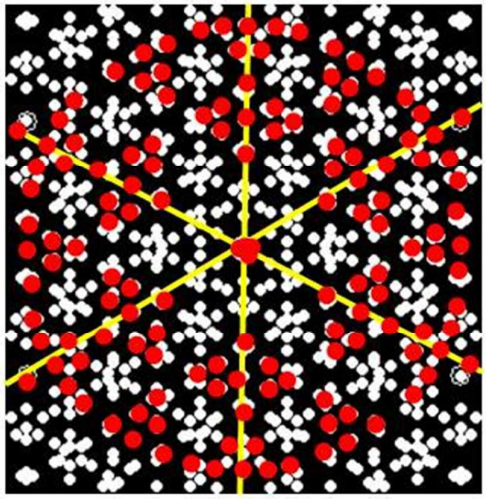

Fig. 7: Comparison between experimental and simulated LEED patterns. Red spots: extracted from the experimental LEED of Fig 3 (c). White spots: from LEEDPat software[31] for a 5x8 superstructure.

C3 Segregation of Ge: As mentioned in the previous section, we conducted evaporations keeping the surface close to RT and around 470 K. For evaporation times corresponding to a few monolayers followed by post annealing at 520 K we obtained LEED patterns similar to those of ref. 9 for both evaporation conditions (Fig. 3(c)). Controlled sputtering of the Ge layer with Ar at low energy (800 eV) allowed us to confirm that the layer grown at RT was slightly thicker. This effect is connected to the fact that Ge migrates into the bulk for temperatures above 400 K, as it was observed for other semiconductor-metal interphases (like Si on Pt[23,32]). This migration of Ge into the bulk limits the rate of growth of the layer, resulting in a thickness that is not linear with the evaporation time. After performing evaporations and post annealing, the following cleaning of the sample to make new fresh layers becomes more difficult because even though the sputtering can remove completely the surface Ge, upon annealing the bulk Ge segregates to the surface giving rise to a new and well-ordered atomic structure (reconstructed structure) containing both Au and Ge atoms. Evidence for this segregation effect is presented in Figure 8. Panel (a) corresponds to TOF-DRS spectra taken along the $[\bar{2}11]$ direction. We observe the already described changes during evaporation, followed by the effect of sputtering which removes the Ge and restores the Au recoil peak, but then, upon annealing to 700 K a Ge recoil peak reappears and is accompanied by a decrease in the Au peak. Spectra measured along the $[\bar{1}01]$ direction (Fig. 8(b)) are also interesting since they show that the sputtering removes completely the Ge layer that contains the incorporated Au atoms, note the complete disappearance of the Au recoil peak along this direction, characteristic of a clean and ordered Au(111) surface. After annealing, the segregation of Ge atoms toward the surface induces the appearance of a Au peak, as it was observed during Ge evaporation. The temperature required to start bringing the Ge atoms to the surface is around 600 K (Fig. 8(c)), however this value seems to depend on the amount of Ge incorporated, and on the cycles of annealing and sputtering that are performed.

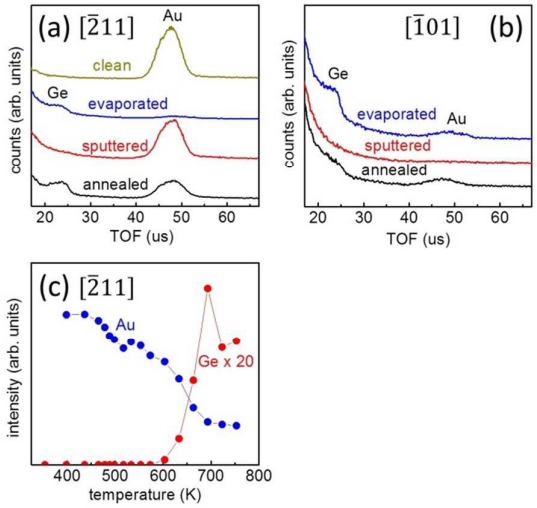

Fig. 8 Effect of segregation: (a) and (b) TOF-DRS spectra recorded at 20° incidence with 4.2 keV Ar^+ ions along the $[\bar{2}11]$ and $[\bar{1}01]$ directions, respectively. (c) Dependence of Au and Ge direct recoil intensities on sample temperature along the $[\bar{2}11]$ direction.

The crystallography of this segregated surface is different from that of the monolayer or the thick layer, and has a composition given by a smaller Ge/Au ratio than that of the higher coverage. Increasing the annealing time or the temperature seems to produce no effect on the well-defined segregated layer. Only by evaporation of additional Ge the segregated layer can evolve further and approach LEED patterns as those of the monolayer or the thick layer (Fig.3).

The corresponding STM images of the segregated surface are shown in Fig. 9 (a) and (b). Note that the structure presents an hexagonal arrangement with very long distances (~4.2nm), with the main distance oriented along the $[\bar{1}01]$ direction. In panel (c) we present a portion of the LEED pattern that shows the 00 and 01 spots. From this pattern it is clearly seen an hexagonal arrangement oriented like the 1x1 Au structure, but with a short distance between spots, i.e., representing a large unit cell. This segregation effect may appear unnoticed because its LEED pattern could be confused with that of the herringbone. A close inspection shows that the points are rotated 30° with respect to those of the herringbone.

In Panel (d) the 2D-FFT of the STM image shown in panel (b) is presented. The measurement of the relative distances between nxn LEED and 2D-FFT spots with respect to the 1x1, together with the distances measured in the STM images, give n of ≈14.

View Article Online
DOI: 10.1039/C7CP02949G

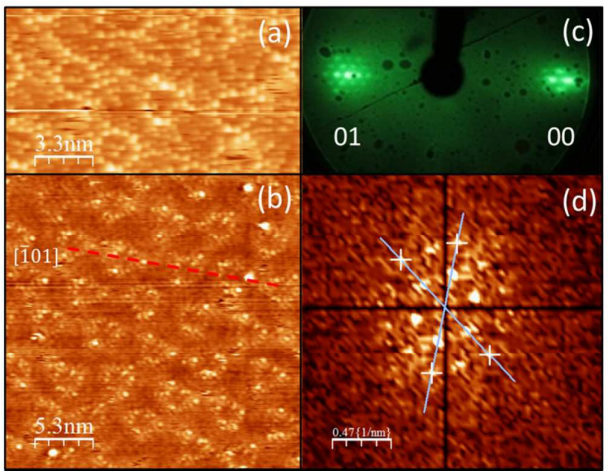

Fig. 9 (a) and (b) STM images acquired with V_S= -0.5 V and I_T = 0.3 nA after segregation of Ge. The red dashed line corresponds to the $[\bar{1}01]$ Au direction. (c) Zoom of the LEED pattern showing the region of the 00 and 01 Au spots. (d) 2D-FFT pattern of image (b) calculated by WSxM software[27].

Conclusions

We prepared Ge films on Au(111) surfaces by *in-situ* evaporation under UHV conditions, following the procedure reported in refs. [9,10]. We followed the adsorption by means of TOF-DRS and LEED techniques, from sub monolayer to a multilayer film. TOF-DRS spectra confirm the coexistence of Ge and Au atoms at the top-most layer of all the films prepared, independent of their thickness. The amount of Ge to Au atoms was roughly estimated to be of the order of 2 for the thicker films. STM shows a complex periodic arrangement compatible with a unit cell of 5x8 (with respect to the Au substrate). The 2D-FFT of the STM images is in good agreement with the experimental LEED pattern.

Attempts to grow multilayers thicker than 4 atomic layers were precluded by the migration of Ge atoms into the bulk. After cleaning the sample, the segregation of the bulk Ge atoms to the surface starts to be observed on the surface at 600 K. This segregation generates an ordered phase having an nxn structure with n~14.

Although the expected honeycomb structure of germanene was not identified clearly we consider that these findings will help to elucidate the complex behavior of Ge films on Au and will provide important information for more realistic models of Ge films on metals.

Acknowledgements

We acknowledge support from U.N. Cuyo (06-C517), ANPCyT (PICT 2012-0124 and PICT-2015-2589) and CONICET (PIP 112-201101-00594 and PIP 112-201501-00274-CO). This work was partially supported by the CNRS French-Argentina International Laboratory for Nanoscience (LIFAN). The computational results presented have been achieved in part using the Centro de Simulación Computacional (CSC) - CONICET.

References

1 A. H. Castro Neto, F. Guinea, N. M. R. Peres, K.S. Novoselov and A.K. Geim, *Rev. Modern Phys.* 2009, **81**, 109.
2 J. Wang, S. Deng, Z. Liu and Z. Liu, *Natl. Sci. Rev.* 2015, **2 (1)**, 22.
3 L. Tao, E. Cinquanta, D. Chiappe, C. Grazianetti, M. Fanciulli, M. Dubey, A. Molle and D. Akinwande, *Nature Nanotechnology* 2015, **10**, 227.
4 S. Kaneko, H. Tsuchiya, Y. Kamakura, N. Mori and M. Ogawa, *Appl. Phys. Express* 2015, **7**, 035102.
5 Y. C. Lin, R. K. Ghosh, R. Addou, N. Lu, S. M. Eichfeld, H. Zhu, M. Y. Li, X. Peng, M. J. Kim, L. J. Li, R. M. Wallace, S. Datta and J. A. Robinson, *Nature Communications* 2015, **6**, 7311.
6 M. Houssa, A. Dimoulas and A. Molle, *J. Phys.: Condens. Matter*, 2015 **27**, 253002.
7 P. Vogt, P. De Padova, Cl. Quaresima, J. Ávila, E. Frantzeskakis, M. C. Asensio, A. Resta, B. Ealet, and Guy Le Lay, *Phys. Rev. Lett.* 2012, **108**, 155501.
8 L. Meng, Y. Wang, L. Zhang, S. Du, R. Wu, L. Li, Y. Zhang, G. Li, H. Zhou, W. A. Hofer, and H. J. Gao, *Nano Lett.*, 2013, ***13*** (2), 685.
9 María E. Dávila and Guy Le Lay, *Scientific Reports* 2016, **6**, 20714.
10 M.E. Dávila, L. Xian, S. Cahangirov, A. Rubio and G. Le Lay, *New J. Phys.* 2014, **16**, 095002.
11 M.A. Ledina, X. Liang, Y.G. Kim, J. Jung, B. Perdue, C. Tsang, M.P. Soriaga and J.L. Stickney. *ECS Transactions* 2015, **66 (6)**, 129.
12 L. Zhang, P. Bampoulis, A.N. Rudenko, Q. Yao, A. van Houselt, B. Poelsema, M.I. Katsnelson and H.J.W. Zandvliet. *Phys. Rev. Lett.* 2016, **116**, 256804.
13 M. Derivaz, D. Dentel, R. Stephan, MC. Hanf, A. Mehdaoui, P. Sonnet and C. Pirri, *Nanoletters* 2015, **15**, 2510.
14 L. Li, S. Lu, J. Pan, Z. Qin, Y. Wang, Y. Wang, G. Cao, S. Du and H. Gao, *Adv. Mater. Comm.* 2014, **26**, 4820.
15 P. Bampoulis, L. Zhang, A. Safaei, R. van Gastel, B. Poelsema and HJ. Zandvliet, *J. Phys Condens. Matter* 2014, **26 (44),** 442001.
16 L. Rast and V.K. Tewary, [cond-mat. mtrl-sci.] 2013 arXiv:1311.0838.
17 W. Xia, W. Hu, Z. Li and Jinlong Yang, *Phys. Chem. Chem. Phys.* 2014, **16**, 22495.
18 A. Acun, L. Zhang, P. Bampoulis, M. Farmanbar, A. van Houselt, A. N. Rudenko, M. Lingenfelder, G. Brocks, B. Poelsema, M. I. Katsnelson and H. J. W. Zandvliet, *J. Phys.: Condens. Matter* 2015, **27**, 443002.
19 H. S. Tsai, Y. Z. Chen, H. Medina, T. Y. Su, T. S. Chou, Y. H. Chen, Y. L. Chueh and J. H. Liang. *Phys. Chem. Chem. Phys.*, 2015, **17** 21389.
20 L. Ruitao , J. A. Robinson, R. E. Schaak, D. Sun, Y. Sun, T. E. Mallouk and M. Terrones. *Acc. Chem. Res.* 2015, **48 (1)**, 56.
21 B. Radisavljevic, A. Radenovic, J. Brivio, V. Giacometti and A. Kis, *Nature Nanotechnology* 2011, **6**, 147.
22 Y. Wang, J. Li, J. Xiong, Y. Pan, M. Ye, Y. Guo, H. Zhang, R. Quhe and J. Lu, *Phys. Chem. Chem. Phys.* 2016, **18**, 19451.
23 M. Švec, P. Hapala, M. Ondráček, P. Merino, M. Blanco-Rey, P. Mutombo, M. Vondráček, Y. Polyak, V. Cháb, J.

View Article Online
DOI: 10.1039/C7CP02949G

A. Martín Gago and P. Jelinek. *Phys. Rev. B* 2014, **89**, 201412(R).
24 J. W. Rabalais, "Principles and Applications of Ion Scattering Spectrometry". Wiley –Interscience Series on Mass Spectroscopy. **2003**. ISBN 0-471-20277-0.
25 O. Grizzi, M. Shi, H. Bu, and J.W. Rabalais, *Rev. Sci. Instrum.* 1990, **61**, 740.
26 Omicron NanoTechnology GmbH, http://www.omicron.de/en/home.
27 I. Horcas, R. Fernández, J. M. Gómez-Rodríguez, J. Colchero, J. Gómez-Herrero, and A. M. Baró, *Rev. Sci. Instrum.* 2007, **78**, 013705.
28 P. Rahe, R. Bechstein, and A. Kühnle, *J. Vac. Sci. Technol. B* 2010, **28 (3)** C4E31-38.
29 Im Langenbroich 20-D-52428 Juelich, Germany, http://www.mateck.de/.
30 A rough estimation of the thickness was obtained from the sputtering time required to remove the Ge layer and reach the substrate: about 50 min with 800 eV Ar ions at a current density of 200 nA/cm^2. The thickness estimation considered a sputtering yield of 1.7, obtained from the SRIM 2008 code. Note that the fluence required to produce sputtering of the layer is 5 - 6 orders of magnitude larger than that used to take the spectra, which confirms the negligible damage during TOF-DRS measurements.
31 K. Hermann, M. A. Van Hove, See: http://w3.rz-berlin.mpg.de/~hermann/LEEDpat/.
32 U Diebold, L. Zhang, J. F. Anderson, and P. Mrozek, *J. Vac. Sci. Technol. A* 1996 **14**, 1679.

View Article Online
DOI: 10.1039/C7CP02949G

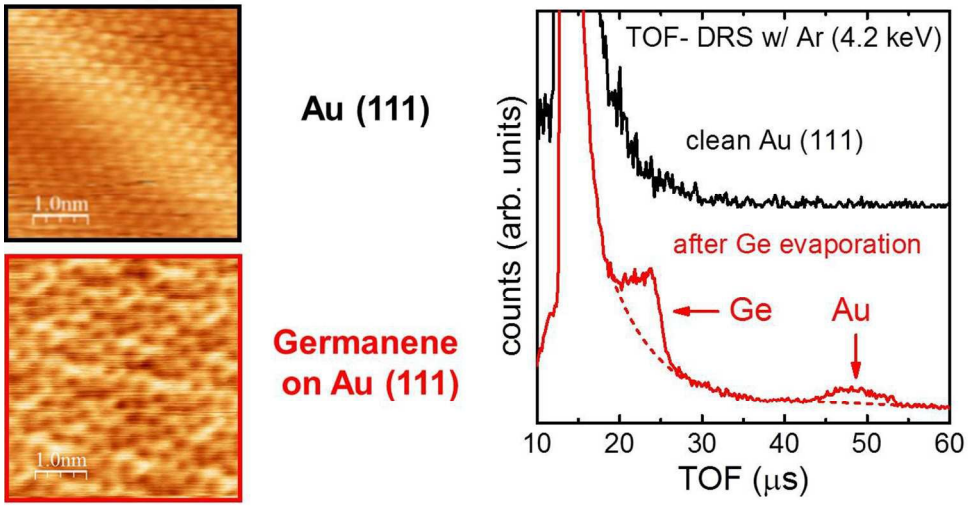

231x119mm (150 x 150 DPI)